



**HAL**  
open science

# Ferroelectric to relaxor crossover in Li solid solutions derived from Ba<sub>2</sub>Nd<sub>2</sub>FeNb<sub>4</sub>O<sub>15</sub>

Thomas Hérisson de Beauvoir, Tom Delage, Michaël Josse

► **To cite this version:**

Thomas Hérisson de Beauvoir, Tom Delage, Michaël Josse. Ferroelectric to relaxor crossover in Li solid solutions derived from Ba<sub>2</sub>Nd<sub>2</sub>FeNb<sub>4</sub>O<sub>15</sub>. *Ceramics International*, 2021, 47 (8), pp.10658-10664. 10.1016/j.ceramint.2020.12.179 . hal-03167134

**HAL Id: hal-03167134**

**<https://hal.science/hal-03167134>**

Submitted on 11 Mar 2021

**HAL** is a multi-disciplinary open access archive for the deposit and dissemination of scientific research documents, whether they are published or not. The documents may come from teaching and research institutions in France or abroad, or from public or private research centers.

L'archive ouverte pluridisciplinaire **HAL**, est destinée au dépôt et à la diffusion de documents scientifiques de niveau recherche, publiés ou non, émanant des établissements d'enseignement et de recherche français ou étrangers, des laboratoires publics ou privés.

# 1 **Ferroelectric to relaxor crossover in Li solid solutions derived from** 2 **Ba<sub>2</sub>Nd□<sub>2</sub>FeNb<sub>4</sub>O<sub>15</sub>**

3 Thomas Hérisson de Beauvoir, Tom Delage, Michaël Josse\*

---

## 4 **Abstract**

5 Three solid solutions of Tetragonal Tungsten Bronze structure containing Li were prepared by solid  
6 state route starting from the parent compound Ba<sub>2</sub>NdFeNb<sub>4</sub>O<sub>15</sub>. These solid solutions involve Li  
7 insertion compensated by cationic removal. All cationic sites were involved to investigate their  
8 influence on the dielectric transitions observed in Ba<sub>2</sub>NdFeNb<sub>4</sub>O<sub>15</sub>, i.e. from relaxor (R) to ferroelectric  
9 (FE) and finally to paraelectric (PE). All solid solutions display the same pattern, which is an evolution  
10 from a relaxor to ferroelectric crossover, leading to a single transition (relaxor to paraelectric). This  
11 evolution is accompanied by a sudden increase of the ordering temperature (T<sub>m</sub>). A focus on structure  
12 refinements shows the slight differences induced by the insertion of Li and points towards the role of  
13 anionic framework as responsible for the dielectric properties of these materials. This study completes  
14 the work performed on other cationic substitutions performed in the title material, and represents a new  
15 example of Li substituted TTb materials.

---

## 16 **Introduction**

17 Materials crystallizing in tungsten bronze structure are of great interest in optical [1,2], dielectric  
18 applications [3–6]. Due to their huge chemical and structural flexibility [7–10], they accommodate most  
19 cation types, but are also able to accommodate various anions and important cationic vacancies [9,11–  
20 16]. TTb structure has been described as a modified perovskite structure that can be written in a general  
21 formula (A1)(A2)<sub>2</sub>C(B1)(B2)<sub>4</sub>O<sub>15</sub> A<sub>2</sub>BC<sub>2</sub>B<sub>1</sub>B<sub>2</sub><sub>4</sub>O<sub>15</sub> made of 2 different octahedral sites (B1 and B2),  
22 arranged in such a way they form channels of 3 different sizes. A sites are pentagonal channels with 15-  
23 coordination. A1 sites stand along the square channels and have a 12-coordination. Finally, the C sites  
24 are distributed in triangular channels where Li<sup>+</sup> ions only seem to fit. They have a 9 coordination and  
25 remain vacant in most TTb materials. The title material Ba<sub>2</sub>NdFeNb<sub>4</sub>O<sub>15</sub> is a parent compound of a

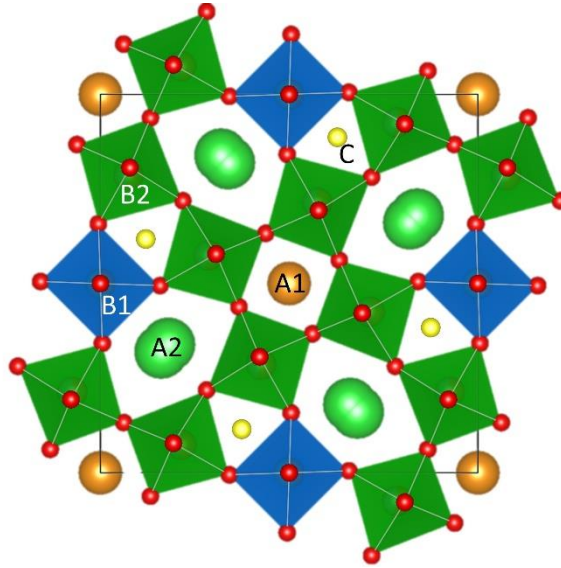
26 wide variety of compositions showing interesting dielectric properties and structural complexity [17–  
27 21]. In this compound, Ba occupies A2 sites, Nd is in the A1 site, while Fe and Nb homogeneously  
28 share the B1 and B2 sites. C sites are therefore empty. Surprisingly, it shows a ferroelectric behavior at  
29 room temperatures while XRD data show an optimal fit with a centrosymmetric space group P4/mbm  
30 [22] along the whole temperature range from ferroelectric to paraelectric temperature domain [23].  
31 Solid solutions based on A1, A2, and B sites substitutions were explored to investigate the dielectric  
32 behaviour and identify the structural modifications inducing it [24,25]. All of them point towards a  
33 similar behavior that was ascribed to oxygen framework. In fact, electron and neutron diffraction  
34 highlighted the subtle modifications of oxygen stacking, probably at the origin of symmetry breaking  
35 inducing ferroelectricity in these TTB materials [23,26]. However, no composition dealing with C sites  
36 were ever derived from the parent Nd-containing TTB. The present paper thus focuses on the influence  
37 of Li addition in  $\text{Ba}_2\text{NdFeNb}_4\text{O}_{15}$  on both dielectric and structural features. Since  $\text{Li}^+$  insertion at C site  
38 induces a modification of global charges in the compound, one has to compensate  $\text{Li}^+$  addition by cation  
39 removal on the other sites. Thus, three different solid solutions were tested to compare the influence of  
40 A1 site, A2 site and B site compensation based on the following patterns (see Figure 1):

- 41 •  $\text{Ba}_2\text{Nd}_{1-x/3}\text{Li}_x\text{FeNb}_4\text{O}_{15}$  (abbreviated NL) in which  $\text{Li}^+$  insertion is compensated by  $\text{Nd}^{3+}$   
42 vacancies in the square channels (A1 site).
- 43 •  $\text{Ba}_{2+x}\text{Nd}_{1-x}\text{Li}_x\text{FeNb}_4\text{O}_{15}$  (abbreviated BNL) in which  $\text{Li}^+$  insertion is compensated by the  
44 substitution of  $\text{Nd}^{3+}$  by  $\text{Ba}^{2+}$  in square channels (A1 site) without introduction of vacancies.
- 45 •  $\text{Ba}_2\text{NdLi}_x\text{Fe}_{1+(x/2)}\text{Nb}_{4-(x/2)}\text{O}_{15}$  (abbreviated LFN) in which  $\text{Li}^+$  insertion is compensated by  
46 changing the  $\text{Fe}^{3+}/\text{Nb}^{5+}$  ratio in octahedral sites, with a limited impact on the TTB framework  
47 as iron and niobium have similar radii.

48 These three substitution pattern should give access to the specific influence of  $\text{Li}^+$  insertion on  
49 dielectric properties, as the various co-substituted ions have been investigated otherwise, including  
50 the influence of  $\text{Nd}^{3+}$  vacancies [27], the influence of  $\text{Nd}^{3+}$  substitution and accommodation of  $\text{Ba}^{2+}$   
51 at the A1 site [23], while the substitution of  $\text{Nb}^{5+}$  by  $\text{Fe}^{3+}$ , the radii of which are very close ( $\text{Nb}^{5+}$ :

52 64 pm; Fe<sup>3+</sup>: 65 pm) allows for the insertion of Li<sup>+</sup> without much modification of the TTB  
53 framework otherwise.

54 In this paper, the study of these three system is presented first, then a focus on the NL system is  
55 developed, before concluding on crystal-chemical considerations concerning the observed  
56 ferroelectric to relaxor crossovers.



57

58 *Figure 1: TTB structure represented along c axis, showing the different cationic sites A1, A2, C, B1 and B2*

## 59 **Experimental section**

60 For all three solid solutions, samples were prepared following the solid state synthesis route, using  
61 BaCO<sub>3</sub> (Cerac 99.9%), Nd<sub>2</sub>O<sub>3</sub> (Cerac 99.9%), Li<sub>2</sub>CO<sub>3</sub> (Sigma-Aldrich 99%), Fe<sub>2</sub>O<sub>3</sub> (Rectapur 99.9%)  
62 and Nb<sub>2</sub>O<sub>5</sub> (LTS chemical 99.95%). To remove hydroxyl groups resulting from hydroxylation of rare  
63 earth oxides, Nd<sub>2</sub>O<sub>3</sub> was heat treated overnight at 1000 °C before use. Powders were weighted and  
64 mixed in targeted stoichiometric quantities, then were hand milled in an agate mortar for 30 min. The  
65 composition ranged between 0 < x < 0.12 for NL, BNL and LFN solid solutions, and were extended up  
66 to x = 0.30 for NL solid solution. The powders were pelletized using a 13 mm diameter die and a  
67 hydraulic press, applying a 200 MPa uniaxial pressure for 1 min. Synthesis was then performed at  
68 1280 °C for 12h, followed by a sintering step at 1310 °C for 10h. Relative densities were measured  
69 geometrically, all being above 95% of theoretical density of each composition.

70 X-ray diffraction data were recorded on a PANalytical X'Pert diffractometer with Bragg-Brentano  
71 geometry (using Cu  $K\alpha_1/K\alpha_2$  radiation) for all composition after synthesis and after sintering on  
72  $8^\circ < 2\theta < 80^\circ$  using a step of  $0.017^\circ$ . For some of the samples for which Rietveld refinements were  
73 conducted, acquisition was performed with a Cu  $K\alpha_1$  radiation and an acquisition range of  $5^\circ$ - $130^\circ$ ,  
74 using a  $0.008^\circ$  step. The pellets' microstructures were observed on surfaces and fractures, with a  
75 scanning electron microscope (JEOL 840 SEM). The microstructure of the ceramics from the BNL and  
76 LFN are not described here, as they were found extremely similar (not to say identical) to that of NL  
77 ceramics (described further in the manuscript). The addition of high contents of Li led to the observation  
78 of some melted part having the same composition as the rest of the sample (see Figure S3). This  
79 phenomenon is observed on the surface of samples but is not visible in the bulk. However, attempts to  
80 sinter during longer dwell times lead to the formation of more of these melted parts, but had no influence  
81 on the measured dielectric properties. Therefore, we will not consider it influences the subsequent  
82 characterizations.

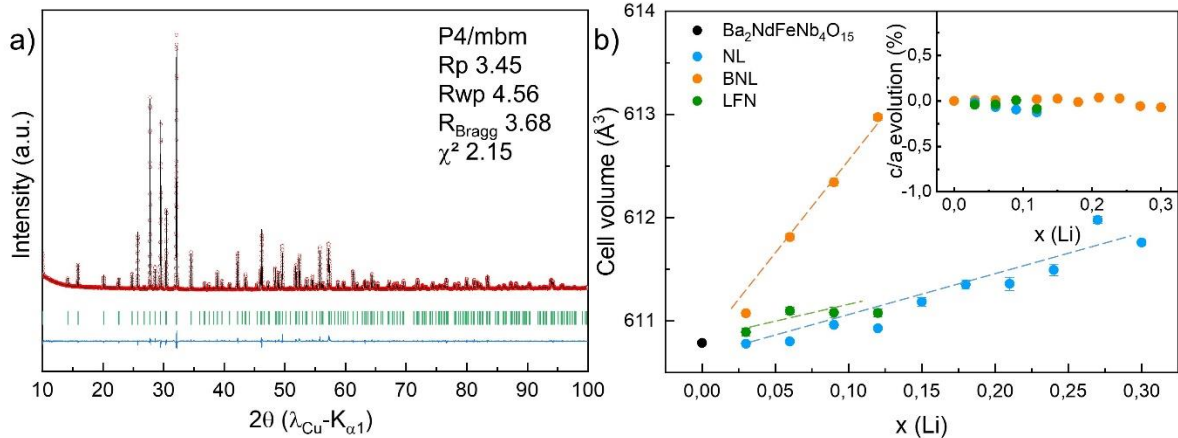
83 The ceramic discs were equipped with sputtered gold electrodes to allow for planar capacitor geometry.  
84 The dielectric measurements were carried out in the frequency range of  $10^3 - 10^6$  Hz (the amplitude of  
85 the applied ac electric field being 1 V) using an HP4194a impedance bridge, at heating rate of  $1^\circ\text{C}/\text{min}$   
86 in a quartz tube filled with He. In some cases, residual water in the measurement setup led to the  
87 observation of a peak, both in real and imaginary part of permittivity, in the range 250-270 K (greyed  
88 areas in figures 3, S1, S2 and S3), which is not considered in the interpretation of the results.

## 89 **Results and discussion**

### 90 *a) Study of NL, BNL and LFN solid solutions*

91 After synthesis, all samples were measured by XRD for the three solid solutions. Rietveld refinement  
92 was performed on parent composition  $\text{Ba}_2\text{NdFeNb}_4\text{O}_{15}$  (Figure 2a) using  $P4/mbm$  space group.

93



94

95 *Figure 2: XRD a) Rietveld refinement of Ba<sub>2</sub>NdFeNb<sub>4</sub>O<sub>15</sub> sintered pellet and b) evolution of lattice volume with sample*  
 96 *composition for the three solid solutions (0 < x < 0.12 for BNL and LFN, and 0 < x < 0.3 for NL solid solutions). Inset*  
 97 *corresponds to c/a lattice parameter ratio of samples for corresponding solid solutions compared to x = 0 sample.*

98 Refinement converged to  $R_{\text{Bragg}} = 3.68$ , confirming the quality of the powder, as well as the absence of

99 secondary phase. Refined lattice size, atomic positions, agitation and occupancies are consistent with

100 previous work published on ceramics and single crystals of the same composition [22,25,27]. Based on

101 these information, one can consider observing the influence of Li addition on the structure. Profile

102 refinements were performed on XRD patterns for all samples of the three solid solutions, and resulting

103 lattice volume is plotted on Figure 2b for NL, BNL and LFN. With increasing x (Li content) in the

104 various solid solutions, two different behaviours can be seen. In the NL and LFN solid solutions, no

105 significant evolution of lattice volume is visible from x = 0 to 0.12, the lattice volume evolving from

106  $610.78(2) \text{ \AA}^3$  to  $610.93(1) \text{ \AA}^3$  for NL and  $611.08(4) \text{ \AA}^3$  for LFN ( $\Delta V_{\text{max}} \approx 0.30(6) \text{ \AA}^3$ , i.e. < 0.1%). On

107 the contrary, in the BNL solid solution, a larger evolution can be observed with a global increase of

108 lattice volume from  $610.78(2) \text{ \AA}^3$  to  $612.97(3) \text{ \AA}^3$  (i.e. 0.36%) when increasing Li content from x = 0

109 to x = 0.12. Increasing x to 0.30 in NL solid solution led to a more significant increase, from

110  $610.93(1) \text{ \AA}^3$  to  $611.76(3) \text{ \AA}^3$  (i.e. 0.14% increase), which can be related to the introduction of vacancies

111 at the A1 site. The corresponding c/a ratio evolution in the three solid solutions remains below 0.1%

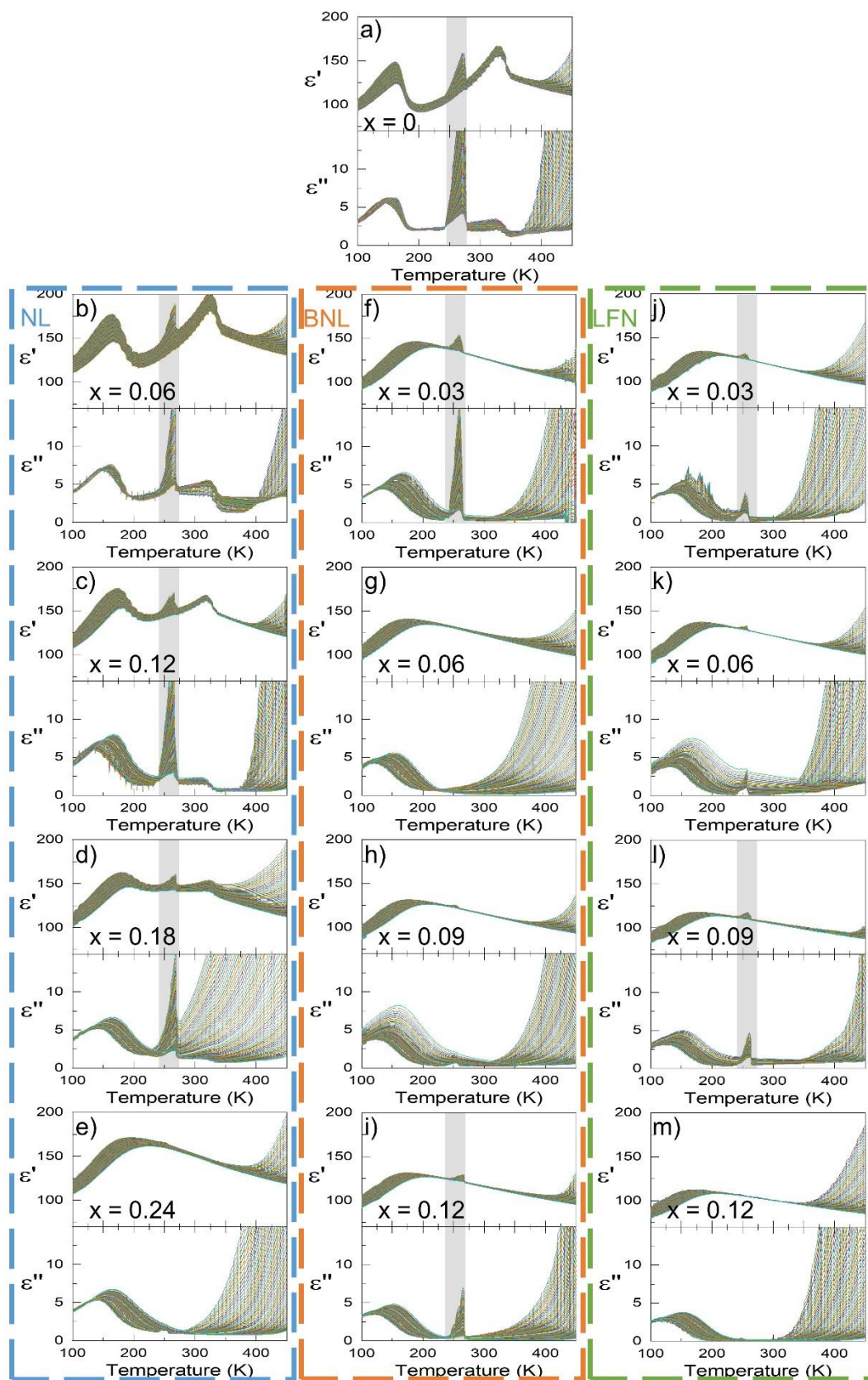
112 difference with x = 0 sample, with no visible trend. In this solid solution (NL), insertion of Li is

113 compensated by removing up to 0.04 Nd when x = 0.12, which corresponds to a formula

114  $\text{Ba}_2\text{Nd}_{0.96}\text{Li}_{0.12}\text{FeNb}_4\text{O}_{15}$ . In this case it means  $\text{Nd}^{3+}$  site occupation is 96 %, which is close to the limit

115 observed for this phase in prior studies [22,23]. In addition, and according to Shannon and Prewitt ionic

116 radii [28],  $\text{Li}^+$  is a very small ion and in a 8-coordinated environment, its size reaches 0.92 Å. Its  
117 apparent size may increase a little in the 9-coordinated environment characteristic of the C sites, but  
118 since only 0.12 Li are added to the phase, the lattice volume evolution must remain very small, as is  
119 observed in the NL system. In LFN solution,  $\text{Li}^+$  insertion is accompanied by a substitution of  $\text{Fe}^{3+}$  for  
120  $\text{Nb}^{5+}$  at octahedral sites, their ionic radii being 0.645 Å and 0.64 Å respectively. Thus, no visible lattice  
121 parameter change is expected from the substitution of  $\text{Fe}^{3+}$  for  $\text{Nb}^{5+}$ . On the opposite, in the case of  
122 BNL solution, for each  $\text{Li}^+$  that is inserted, one  $\text{Ba}^{2+}$  ion is substituted for an  $\text{Nd}^{3+}$  ion. Since the A2 site  
123 is fully occupied by  $\text{Ba}^{2+}$  ions, the substituted ones must be inserted at the A1 site, a substitution scheme  
124 that was confirmed by Pierre Heijboer in his study of the  $\text{Ba}_{6-2x}\text{Nd}_{2x}\text{Fe}_{2+x}\text{Nb}_{8-x}\text{O}_{30}$  solid solution [23].  
125 As  $\text{Ba}^{2+}$  ionic radius reaches 1.61 Å, and taking into account that  $\text{Nd}^{3+}$  ionic radius is 1.27 Å -  
126 considering 12-coordination [28] - the substitution of  $\text{Nd}^{3+}$  by  $\text{Ba}^{2+}$  must result in a significant increase  
127 of lattice volume. Then, one can conclude that the evolution of lattice volume determined from PXRD  
128 seem to be consistent with what can be expected from crystal-chemical considerations.

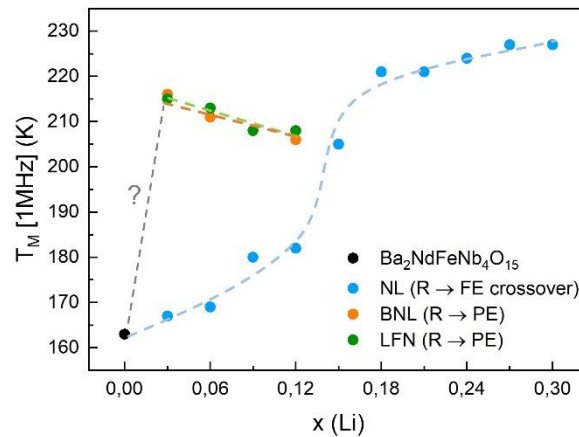


129

130  
131

Figure 3: Dielectric measurements of a)  $\text{Ba}_2\text{NdFeNb}_4\text{O}_{15}$  then (b-e) NL, (f-i) BNL and (j-m) LFN solid solutions. Greyed areas indicate spurious contributions from residual water (see experimental section).

132 Dielectric measurements were then performed for all compositions and some of them are displayed on  
 133 Figure 3 for the NL solid solution (see Figures S1 for the complete set of NL measurements). For  $x$  up  
 134 to 0.12, they confirm the high quality of different samples since dielectric losses remain very low below  
 135 400 K. One can notice a double transition in  $x = 0$  composition ( $\text{Ba}_2\text{NdFeNb}_4\text{O}_{15}$ ), showing a relaxor  
 136 behavior at low temperature, followed by a ferroelectric phase transition around 160 K, and finally a  
 137 paraelectric phase transition at 330 K. This is consistent with the relaxor (R) to ferroelectric (FE)  
 138 crossovers previously observed in this composition [24,25,29,30] and confirms the quality of samples  
 139 obtained. The general trend for the three different solid solutions is the transition from a R-FE crossover  
 140 to a purely relaxor behavior with Li addition, which is consistent with the data obtained for other  
 141 systems derived from  $\text{Ba}_2\text{NdFeNb}_4\text{O}_{15}$ . However, the Li content inducing a modification in the  
 142 dielectric behavior is very different between NL solid solution and the two others. Although R-FE  
 143 crossover is observed for  $x < 0.24$  in NL, both BNL and LFN switch to R behavior for the lowest Li  
 144 content explored ( $x=0.03$ ). This drastic modification of the dielectric behaviour is accompanied by more  
 145 subtle changes.



146

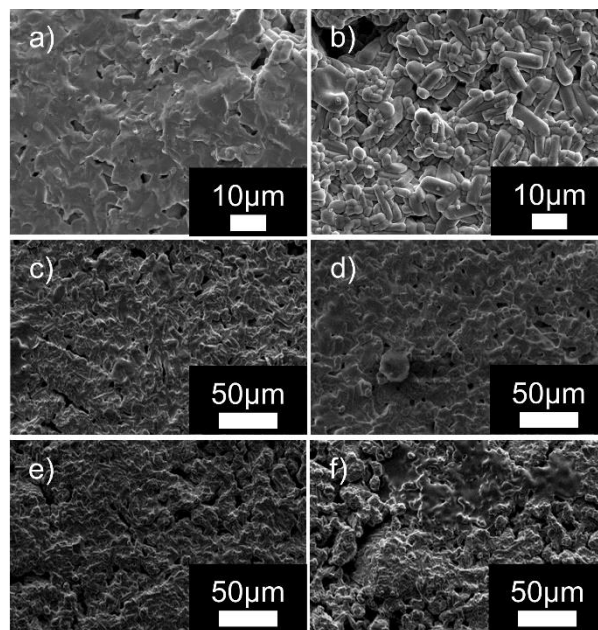
147 *Figure 4: Dielectric transition temperature associated to R→FE and R→PE phase transition at 1 MHz for various solid*  
 148 *solutions*

149 Figure 4 displays the transition to relaxor state ( $T_M$ ) for various samples tested. On the one hand, in both  
 150 BNL and LFN,  $T_M$  occurs at a relatively stable but higher temperature ( $\sim 210$ - $215$  K) for  $0.03 < x < 0.12$ ,  
 151 i.e. almost 40 K above the transition observed in the unsubstituted Nd TTB ( $x = 0$ ,  $T_M \approx 160$  K). On the  
 152 other hand, for NL,  $T_M$  rises up smoothly with increasing  $x$ , up to  $\sim 180$  K for  $x = 0.12$ . The case of NL

153 is quite specific since two major steps appear: i) while  $x < 0.15$ ,  $T_M$  evolves linearly between 160 and  
154 180 K, ii) for  $x > 0.18$ , evolution is still linear but above 200 K, associated with a pure R behaviour. In  
155 between these two steps, a jump in  $T_M$  occurs, which is accompanied by a disappearance of F transition  
156 ( $0.15 < x < 0.21$ ) (see Figure S1 for details).

157 The question then arises about the behaviour of these two solid solutions at smaller Li content, as  
158 compared with NL evolution. In the BNL solid solution introduction of  $Ba^{2+}$  ions at the A1 site  
159 obviously put severe strain on the TTB framework, as illustrated by the cell volume evolution, while if  
160 in LFN solid solution the cell volume is stable, the compensation involves the ferroelectrically active  
161 Nb sublattice. To further understand these behaviours, exploring smaller Li substitution rates would be  
162 necessary, unfortunately, our experimental conditions prevented us from doing so with accuracy. For  
163 these reasons, it appears interesting to focus on the NL solid solution to try to identify the relationship  
164 between ferroelectric to relaxor crossover, crystal structure and Li insertion at the C site. Moreover, the  
165 NL solid solution induces minor lattice size evolution (see Figure 2b), which should be an advantage to  
166 detect the subtle crystalline modification at the origin of the dielectric behavior evolution.

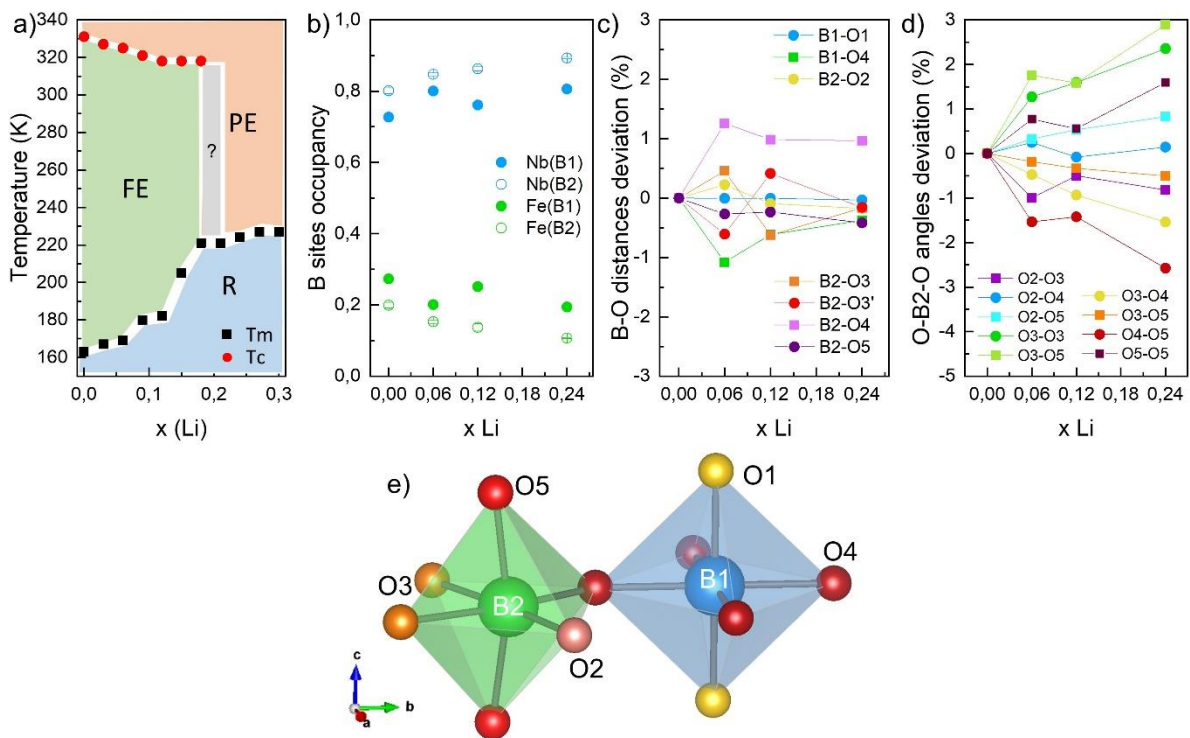
167 b) *Extended study of NL solid solution*



168

169 *Figure 5: SEM images of NL solid solution samples a) fracture of  $x = 0$  and surfaces of b)  $x = 0$ , c)  $x = 0.03$ , d)  $x = 0.06$ , e)*  
170  *$x = 0.09$  and f)  $x = 0.12$*

171 Figure 5 shows SEM images of samples from NL solid solution with  $x$  from 0 to 0.12. As shown here,  
 172 grains have a rod like shape for the various contents of Li and show no explicit morphology evolution  
 173 that could be connected to the evolution of their dielectric properties. Moreover, it seems that Li, as a  
 174 very mobile ion, does not influence grain growth as it could be expected. All samples show a dense  
 175 microstructure consistent with the geometrically measured densities, all above 95% of theoretical  
 176 density.



177

178 *Figure 6: Dielectric analyses of NL solid solution: a) dielectric phase diagram showing  $T_c$  and  $T_m$  (at 1 MHz) delimitating*  
 179 *three domains: FE(ferroelectric), R (relaxor) and PE (paraelectric), b) octahedral B1 and B2 site occupancy, c) normalized*  
 180 *B-O distances in B1-O and B2-O and d) normalized O-B-O bond angles in B2 site distorted octahedron (error bars are*  
 181 *presented but remain below symbols for some data, but these errors arise from the quality of fit, which do not correspond to*  
 182 *the actual resolution of data). e) Representation of B1 and B2 sites with their neighboring oxygen environment*

183 Based on dielectric measurements (Figure 3 and Figure S1), it was possible to draw a dielectric phase  
 184 diagram for NL solid solution (see Figure 6a) showing 3 dielectric domains (ferroelectric, paraelectric  
 185 and relaxor). Two different kinds of responses appear in these measurements. For small Li contents,  
 186  $0 \leq x \leq 0.18$ , two distinct dielectric anomalies are observed. The low temperature one (around 200 K)  
 187 has a maximum that is frequency dependent, whereas the second one around 330 K is frequency  
 188 independent. They respectively correspond to relaxor (R)  $\rightarrow$  ferroelectric (FE) and ferroelectric (FE)  
 189  $\rightarrow$  paraelectric (PE) phase transitions and thus a relaxor to ferroelectric crossover is found in this region

190 of the dielectric phase diagram. For larger Li contents, only a R  $\rightarrow$  PE transition is observed, and this  
191 global behavior is similar to that of others solid solutions derived from Ba<sub>2</sub>NdFeNb<sub>4</sub>O<sub>15</sub> [22–26]. In  
192 addition, for  $x > 0.03$ , the amplitude of the FE transition decreases with increasing Li content, while that  
193 of the R transition seems to reach a plateau. To investigate the relationship between this observation  
194 and the crystalline phase, Rietveld refinements were performed on 4 samples of the solid solution,  
195 namely  $x = 0, 0.06, 0.12$  and  $0.24$ . Refinements results are displayed on Figure S2, along with  
196 agreement factors. Refined atomic parameters are summarized in Table S1. These refinements confirm  
197 the quality of samples and the absence of secondary phases. Nb<sup>5+</sup> being the d<sup>0</sup> ion in the central position  
198 of octahedrons can be considered as the ferroelectrically active ion in the structure. While in the present  
199 case, it may not be the actual driving force for ferroelectricity [24,27,31,32], it appears interesting to  
200 have a look at its environment. These are summarized for the different samples in Figure 6b to d. TTB  
201 structure contains 2 different octahedral sites, named B1 and B2, corresponding to regular (B1) and  
202 distorted (B2) sites.

203 The distribution of Fe and Nb on the B1 and B2 sites (Figure 6b) seems to be random, with Fe occupying  
204 ~20% of both B1 and B2, while Nb occupies ~80%. Nonetheless, it appears that Fe is slightly more  
205 stable in B1 site than B2, since about 5% higher content is found in the four samples measured. The  
206 statistical distribution tends to be stable for samples with  $x < 0.2$ , but slightly changes in the case of  
207  $x = 0.24$ . The refinement result gives a site occupancy  $> 80\%$  for Nb in B1 and  $> 90\%$  in B2. This is  
208 not consistent with the stoichiometry of the starting powders (Nb content is 80% maximum), but must  
209 be related to a modification in the octahedral environment that cannot be resolved from our experimental  
210 data.

211 Figure 6c shows the evolution of B-O bond distance in both octahedrons normalized to the B-O  
212 distances in  $x = 0$ . This plot shows that although there is a slight increase of B2-O4 distance for the  
213 sample  $x = 0.24$ , the same phenomenon is observed for the two intermediate compositions 0.06 and  
214 0.12. Therefore it is not sufficient to explain the observations made in dielectric measurements.  
215 Regarding the other distances, it is quite surprising to notice that no significant difference is observed  
216 between  $x = 0$  (RF) and  $0.24$  (R) that could be related to the occurrence of ferroelectric transition.

217 Moreover, if one excludes B2-O4 distance, B-O distances are closer between  $x = 0$  and  $x = 0.24$  than  
218 between  $x = 0$  and  $x = 0.06$  or  $0.12$ . These observations indicate that insertion of Li at the C site does  
219 not induce modification of bond lengths at the B1 and B2 sites that could be detected through  
220 conventional 3D crystallography. As the title material is prone to aperiodic modulations, Li insertion  
221 may only affect these modulations, which are related to dielectric behaviour [10], and induce the  
222 observed ferroelectric to relaxor crossover.

223 Concerning O-B2-O angles of the distorted octahedron, (Figure 6d) one can see that a global increase  
224 is observed from  $x = 0$  to  $0.24$ . The maximum evolution for  $x = 0.06$  and  $x = 0.12$  is limited to 1.5-2%  
225 while it increases to almost 2.5-3% for  $x = 0.24$ , for O3 and O5 sites. These two sites were already  
226 highlighted as showing a strongly anisotropic displacement for  $\text{Ba}_2\text{LnFeNb}_4\text{O}_{15}$  (Ln = Pr, Nd, Sm, Eu)  
227 single crystals, which crystal structures were refined in P4/mbm space group [33]. We also highlighted  
228 in previous works clues of in-plane antiferroelectric dipolar moments in similar compounds, both in  
229 solid ceramics and single crystals [30,33–35]. This highlights the global off-centering of the ion in B2,  
230 which is confirmed by the increase of O5-B2-O5 angle with  $x(\text{Li})$ . Thus it seems that introduction of  
231 lithium enhances the ferroelectric distortion in  $\text{Ba}_2\text{NdFeNb}_4\text{O}_{15}$ , but simultaneously results in the  
232 disappearance of the ferroelectric state. This might originate from a competition between in-plane  
233 antiferroelectric and out-of-plane ferroelectric dipoles [30]. These contradictory observations, however,  
234 are mitigated by the fact that the aforementioned off-centering is an in-plane displacement. Since a 4-  
235 fold axis lies along the  $c$  axis, a displacement in the  $ab$  plane of B2 cation must result in an antiparallel  
236 arrangement of dipoles, which should be associated with an antiferroelectric behaviour obviously  
237 [30,36]. Since a ferroelectric behaviour is observed for  $x$  up to  $0.18$  while the off-centering is maximized  
238 for  $x=0,24$ , the dielectric signature in this system may be the result of competing ferroelectric and  
239 antiferroelectric states related to a subtle distortion mechanism.

240 Indeed, previous work highlighted the presence of a structural aperiodic modulation in  $\text{Ba}_2\text{NdFeNb}_4\text{O}_{15}$ ,  
241 and previous work on the exploration of solid solutions showed that it most likely affects the oxygen  
242 framework [24]. Structure refinement on  $\text{Ca}_{0.28}\text{Ba}_{0.72}\text{Nb}_2\text{O}_6$  has been performed on single crystals, and  
243 can also be refined in a P4/mbm space group. However, its refinement was done considering an

244 aperiodic modulation using the space group  $X4bm(AA0, -AA0)$  [31]. This showed that oxygen  
245 positions are strongly affected by the modulation, with a maximum position shift up to  $0.2 \text{ \AA}$ , resulting  
246 in a cooperative octahedral tilting mainly affecting B2 sites. Thus, B2 cations are also strongly affected  
247 by the octahedral displacement, which is suspected to give rise to polarization. Our present  
248 observations, along with the observations of incommensurate modulations in  $Ba_2NdFeNb_4O_{15}$  [24] thus  
249 tend to confirm that the anionic framework constitutes the main driving force of the dielectric behaviour  
250 of these TTB, and that the observation of large atomic displacement parameters for oxygen ions (Table  
251 S1) must be regarded as a signature of a structural modulation. Indeed, a relaxor to ferroelectric  
252 crossover has now been observed from cationic substitutions in any of the cationic sites of the TTB  
253 framework, with strikingly similar dielectric phase diagrams [24]. Further work has to be conducted on  
254 the structural modulation of these materials for a deeper understanding of the crystallographic origin of  
255 ferroelectric properties observed.

## 256 **Conclusion**

257 Li-substituted TTB materials derived from the composition  $Ba_2dFeNb_4O_{15}$  were successfully prepared  
258 following three composition patterns, namely NL, BNL and LFN. All substitution scheme allowed for  
259 Li accommodation in TTB structure without secondary phase formation. Addition of Lithium in the  
260 structure led to the modification of dielectric properties from a relaxor (R)  $\rightarrow$  ferroelectric (FE)  $\rightarrow$   
261 paraelectric (PE) crossover to a single (R)  $\rightarrow$  (PE) phase transition. In the BNL and LFN systems, this  
262 modification is observed for the smallest substitution rates investigated. In NL, this modification  
263 requires larger amounts of Li ( $x > 0.2$ ) and comes along with an increase of (R)  $\rightarrow$  (FE) transition  
264 temperature ( $T_m$ ) as compared to parent compound  $Ba_2NdFeNb_4O_{15}$ . Rietveld refinements on sintered  
265 pellets were performed in order to identify the structural evolution induced by the insertion of Li  
266 responsible for the dielectric evolution. Detailed analyses of atomic parameters, bond distances and  
267 angles, but also site occupancy or isotropic displacements parameters do not allow to decipher the  
268 mechanism related to a modified dielectric behavior. The present study complete the range of cationic  
269 substitution inducing relaxor to ferroelectric crossovers in  $Ba_2NdFeNb_4O_{15}$ -derived TTB. With  
270 advanced dielectric characterizations previously establishing the existence of a metastable ferroelectric

271 phase [30], these TTB form a highly versatile, highly tunable family of dielectric materials, in which  
272 subtle crystallographic evolutions influence relaxor and ferroelectric phase formation. Further  
273 investigations are needed to clearly link the observed structural modulation of some TTB compounds  
274 to their dielectric behavior evolution, especially Fe containing TTB materials.

## 275 **References**

- 276 [1] P. V. Lenzo, E.G. Spencer, A.A. Ballman, Electro-optic coefficients of ferroelectric strontium  
277 barium niobate, *Appl. Phys. Lett.* 11 (1967) 23–24. doi:10.1063/1.1754944.
- 278 [2] L.G. Van Uitert, S. Singh, H.J. Levinstein, J.E. Geusic, W.A. Bonner, A new and stable  
279 nonlinear optical material, *Appl. Phys. Lett.* 11 (1967) 161–163. doi:10.1063/1.1755079.
- 280 [3] R.J. Xie, Y. Akimune, K. Matsuo, T. Sugiyama, N. Hirosaki, T. Sekiya, Dielectric and  
281 ferroelectric properties of tetragonal tungsten bronze  $\text{Sr}_{2-x}\text{Ca}_x\text{NaNb}_5\text{O}_{15}$  ( $x=0.05-0.35$ )  
282 ceramics, *Appl. Phys. Lett.* 80 (2002) 835–837. doi:10.1063/1.1446997.
- 283 [4] M.C. Stennett, G.C. Miles, J. Sharman, I.M. Reaney, A.R. West, A new family of ferroelectric  
284 tetragonal tungsten bronze phases,  $\text{Ba}_2\text{MTi}_2\text{X}_3\text{O}_{15}$ , *J. Eur. Ceram. Soc.* 25 (2005) 2471–2475.  
285 doi:10.1016/j.jeurceramsoc.2005.03.198.
- 286 [5] I. Levin, M.C. Stennett, G.C. Miles, D.I. Woodward, A.R. West, I.M. Reaney, Coupling between  
287 octahedral tilting and ferroelectric order in tetragonal tungsten bronze-structured dielectrics,  
288 *Appl. Phys. Lett.* 89 (2006) 122908.
- 289 [6] J.A. McNulty, T.T. Tran, P.S. Halasyamani, S.J. McCartan, I. MacLaren, A.S. Gibbs, F.J.Y.  
290 Lim, P.W. Turner, J.M. Gregg, P. Lightfoot, F.D. Morrison, An Electronically Driven Improper  
291 Ferroelectric: Tungsten Bronzes as Microstructural Analogs for the Hexagonal Manganites,  
292 *Adv. Mater.* 31 (2019) 1–9. doi:10.1002/adma.201903620.
- 293 [7] J. Ravez, H. El Alaoui-Belghiti, M. Elaouadi, A. Simon, Relations between ionic order or  
294 disorder and classical or relaxor ferroelectric behaviour in two lead-free TKWB-type ceramics,  
295 *Mater. Lett.* 47 (2001) 159–164. doi:10.1016/S0167-577X(00)00228-7.
- 296 [8] A. Aydi, H. Khemakhem, C. Boudaya, A. Simon, R. Von Der Mühl, X-ray and dielectric studies  
297 of ferroelectric or relaxor phases in the  $\text{Ca}_{1-x}\text{Na}_x\text{Sn}_{1-x}\text{Nb}_x\text{O}_3$  system, *Solid State Sci.* 7 (2005)  
298 249–255. doi:10.1016/j.solidstatesciences.2004.10.009.
- 299 [9] J. Gardner, F.D. Morrison, A-site size effect in a family of unfilled ferroelectric tetragonal  
300 tungsten bronzes:  $\text{Ba}_4\text{R}_{0.67}\text{Nb}_{10}\text{O}_{30}$  ( $\text{R} = \text{La, Nd, Sm, Gd, Dy and Y}$ ), *Dalt. Trans.* 43 (2014)  
301 11687. doi:10.1039/C4DT00126E.
- 302 [10] X. Zhu, M. Fu, M.C. Stennett, P.M. Vilarinho, I. Levin, C.A. Randall, J. Gardner, F.D. Morrison,  
303 I.M. Reaney, A Crystal-chemical framework for relaxor versus normal ferroelectric behavior in  
304 tetragonal tungsten bronzes, *Chem. Mater.* 27 (2015) 3250–3261.  
305 doi:10.1021/acs.chemmater.5b00072.
- 306 [11] A. Rotaru, F.D. Morrison, Vogel-Fulcher analysis of relaxor dielectrics with the tetragonal  
307 tungsten bronze structure:  $\text{Ba}_6\text{M}\text{Nb}_9\text{O}_{30}$  ( $\text{M} = \text{Ga, Sc, In}$ ), *J. Therm. Anal. Calorim.* 120 (2015)  
308 1249–1259.
- 309 [12] J. Gardner, F.D. Morrison, Manipulation of polar order in the “empty” tetragonal tungsten  
310 bronzes:  $\text{Ba}_{4-x}\text{Sr}_x\text{Dy}_{0.67}\text{Nb}_{10}\text{O}_{30}$ ,  $x = 0, 0.25, 0.5, 1, 2, 3$ , *Appl. Phys. Lett.* 109 (2016)  
311 0–5. doi:10.1063/1.4960712.

- 312 [13] J. Gardner, F. Yu, C. Tang, W. Kockelmann, W. Zhou, F.D. Morrison, Relaxor-to-Ferroelectric  
313 Crossover and Disruption of Polar Order in “Empty” Tetragonal Tungsten Bronzes, *Chem.*  
314 *Mater.* 28 (2016) 4616–4627.
- 315 [14] Q. Li, F.-Z. Yao, Y. Liu, G. Zhang, H. Wang, Q. Wang, High-Temperature Dielectric Materials  
316 for Electrical Energy Storage, *Annu. Rev. Mater. Res.* 48 (2018) 3.1-3.25.
- 317 [15] Z. Guo, S. Wu, C. Hu, L. Liu, L. Fang, Preparation and dielectric properties of  
318  $Ba_4RFe_{0.5}Nb_{9.5}O_{30}$  ( $R = La, Nd, Eu, Gd$ ) unfilled tungsten bronze ceramics, *J. Alloys Compd.*  
319 773 (2019) 470–481. doi:10.1016/j.jallcom.2018.09.241.
- 320 [16] S. Wu, C. Sun, X. Yang, C. Hu, L. Liu, L. Fang, Effect of strontium substitution on the structure  
321 and dielectric properties of unfilled tungsten bronze  $Ba_{4-x}Sr_xSmFe_{0.5}Nb_{9.5}O_{30}$  ceramics,  
322 *Ceram. Int.* 46 (2020) 9240–9248. doi:10.1016/j.ceramint.2019.12.177.
- 323 [17] T. Hajlaoui, M. Josse, C. Harnagea, A. Pignolet, Tetragonal tungsten bronze  $Ba_2EuFeNb_4O_{15}$ –  
324 based composite thin films multiferroic at room temperature, *Mater. Res. Bull.* 86 (2017) 30–  
325 37. doi:10.1016/j.materresbull.2016.10.004.
- 326 [18] R. Bodeux, D. Michau, M. Maglione, M. Josse, Thin films sputtered from  $Ba_2NdFeNb_4O_{15}$   
327 multiferroic targets on  $BaFe_{12}O_{19}$  coated substrates, *Mater. Res. Bull.* 81 (2016) 49–54.  
328 doi:10.1016/j.materresbull.2016.04.027.
- 329 [19] F. Roulland, M. Josse, E. Castel, M. Maglione, Influence of ceramic process and Eu content on  
330 the composite multiferroic properties of the  $Ba_{6-2x}Ln_{2x}Fe_{1+x}Nb_{9-x}O_{30}$  TTB system, *Solid*  
331 *State Sci.* 11 (2009) 1709–1716. doi:10.1016/j.solidstatesciences.2009.05.031.
- 332 [20] W. Chen, W.Z. Yang, X.Q. Liu, X.M. Chen, Structural, dielectric and magnetic properties of  
333  $Ba_3SrLn_2Fe_2Nb_8O_{30}$  ( $Ln = La, Nd, Sm$ ) filled tungsten bronze ceramics, *J. Alloys Compd.*  
334 675 (2016) 311–316. doi:10.1016/j.jallcom.2016.03.099.
- 335 [21] T.T. Gao, W. Chen, X.N. Zhu, X.L. Zhu, X.M. Chen, Dielectric and ferroelectric characteristics  
336 of  $Ba_4Pr_2Fe_2Nb_8O_{30}$  tungsten bronze ceramics, *Mater. Chem. Phys.* 181 (2016) 47–53.  
337 doi:10.1016/j.matchemphys.2016.06.032.
- 338 [22] E. Castel, Synthèse de nouveaux matériaux multiferroïques au sein de la famille des bronzes  
339 quadratiques de formule  $Ba_2LnFeNb_4O_{15}$ , University of Bordeaux, 2009.
- 340 [23] P. Heijboer, Etude des propriétés diélectriques et structurales de monocristaux et céramiques de  
341 structure TTB, University of Bordeaux, 2014.
- 342 [24] M. Josse, P. Heijboer, M. Albino, F. Molinari, F. Porcher, R. Decourt, D. Michau, E. Lebraud,  
343 P. Veber, M. Velazquez, M. Maglione, Original Crystal-Chemical Behaviors in  
344  $(Ba,Sr)_2Ln(Fe,Nb,Ta)_5O_{15}$  Tetragonal Tungsten Bronze: Anion-Driven Properties Evidenced  
345 by Cationic Substitutions, *Cryst. Growth Des.* 14 (2014) 5428–5435.
- 346 [25] E. Castel, M. Josse, D. Michau, M. Maglione, Flexible relaxor materials:  $Ba_2Pr(x)Nd_{(1-x)}$   
347  $FeNb_4O_{15}$  tetragonal tungsten bronze solid solution., *J. Physics. Condens. Matter.* 21  
348 (2009) 452201. doi:10.1088/0953-8984/21/45/452201.
- 349 [26] M. Albino, Synthèse et caractérisation structurale et diélectrique de céramiques et de  
350 monocristaux relaxeurs de structure TTB, Université de Bordeaux, 2013.
- 351 [27] M. Albino, P. Veber, S. Pechev, M. Maglione, Growth and Characterization of  $Ba_2LnFeNb_4$   
352  $O_{15}$  ( $Ln = Pr, Nd, Sm, Eu$ ) Relaxor Single Crystals, *Cryst. Growth Des.* 14 (2014) 500–512.
- 353 [28] R.D. Shannon, C.T. Prewitt, Effective ionic radii in oxides and fluorides, *Acta Crystallogr. Sect.*  
354 *B Struct. Crystallogr. Cryst. Chem.* 25 (1969) 925–946.
- 355 [29] M. Josse, O. Bidault, F. Roulland, E. Castel, A. Simon, D. Michau, R. Von der Mühl, O.  
356 Nguyen, M. Maglione, The  $Ba_2LnFeNb_4O_{15}$  “tetragonal tungsten bronze”: Towards RT

- 357 composite multiferroics, *Solid State Sci.* 11 (2009) 1118–1123.
- 358 [30] M. Albino, P. Heijboer, F. Porcher, R. Decourt, P. Veber, M. Maglione, M. Josse, Metastable  
359 ferroelectric phase and crossover in the  $\text{Ba}_2\text{NdFeNb}_{4-x}\text{Ta}_x\text{O}_{15}$  TTB solid solution, *J. Mater.*  
360 *Chem. C.* 6 (2018) 1521–1534. doi:10.1039/C7TC04742H.
- 361 [31] H. a. Graetsch, C.S. Pandey, J. Schreuer, M. Burianek, M. Mühlberg, Incommensurate  
362 modulation of calcium barium niobate (CBN28 and Ce:CBN28), *Acta Crystallogr. Sect. B*  
363 *Struct. Sci.* 68 (2012) 101–106.
- 364 [32] H. a. Graetsch, J. Schreuer, M. Burianek, M. Mühlberg, Thermally induced structural changes  
365 in incommensurate calcium barium niobate  $\text{Ca}_{0.28}\text{Ba}_{0.72}\text{Nb}_2\text{O}_6$  (CBN28), *J. Solid State*  
366 *Chem.* 196 (2012) 255–266.
- 367 [33] M. Albino, P. Veber, E. Castel, M. Velázquez, K. Schenk, G. Chapuis, M. Lahaye, S. Pechev,  
368 M. Maglione, M. Josse, Growth and Characterization of Centimeter-Sized  $\text{Ba}_2\text{LaFeNb}_4\text{O}_{15}$   
369 Crystals from High-Temperature Solution under a Controlled Atmosphere, *Eur. J. Inorg. Chem.*  
370 (2013) 2817–2825.
- 371 [34] P. Heijboer, Etude des propriétés diélectriques et structurales de monocristaux et céramiques de  
372 structure TTB, (2014).
- 373 [35] M. Albino, Synthèse et caractérisation structurale et diélectrique de céramiques et de  
374 monocristaux relaxeurs de structure TTB, University of Bordeaux, 2013.
- 375 [36] H. Amorín, J. Pérez, A. Fundora, J. Portelles, F. Guerrero, M.R. Soares, E. Martínez, J.M.  
376 Siqueiros, Evidence of short-range antiferroelectric local states in lanthanum- and titanium-  
377 modified  $\text{Sr}_{0.3}\text{Ba}_{0.7}\text{Nb}_2\text{O}_6$  ferroelectric ceramics, *Appl. Phys. Lett.* 83 (2003) 4390–4392.  
378 doi:10.1063/1.1629377.
- 379